Journal of Supramolecular Structure 10:1–11 (1979)

Proteolytic Cleavage and Structural Transformation: Their Relationship in Bacteriophage T4 Capsid Maturation

Alasdair C. Steven and Jose L. Carrascosa

Department of Microbiology, Biozentrum der Universität Basel, Klingelbergstrasse 70, CH-4056 Basel, Switzerland

Giant T4 phage capsoids formed in canavanine-treated cultures infected by phage mutants in genes 21 and 17, respectively, differ with regard to cleavage of the major capsid protein, gp23, and in the fine structure of their hexagonal surface lattices. Quantitative computer processing of electron micrographs shows that the significant differences in capsomer morphology amount to six symmetrically placed features present in the uncleaved hexamer but absent after cleavage. These features may be related with the N-terminal portions of gp23 monomers excised by phage-specific proteolysis. Cleaved 17⁻ giants can be induced to undergo a further structural transformation (expansion). Structural characteristics of partially transformed giant particles give clues about the dynamics of the cleavage and expansion transformations. Both processes appear to be polar, initiating in one cap and propagating along the particle. The transition zone of partial cleavage is diffuse, whereas the transition between unexpanded and expanded areas is confined to a narrow band of some 20 nm width.

Key words: **virus assembly, limited proteolysis, conformational change, cooperativity, electron microscopy, optical diffraction, computer image processing**

Limited proteolysis, a versatile mechanism of biological regulation [1, 2], has recently been found to participate in complex assembly reactions such as cell membrane biogenesis [3, 4] and virus assembly [5, 6]. The assembly pathway of bacteriophage T4 head, one of the earliest viral systems in which proteolytic reactions were observed [7–10], has since been studied intensively. This pathway proceeds by the initial formation of a precursor

Dr. Steven is now at Laboratory of Physical Biology, National Institute of Arthritis, Metabolism, and Digestive Diseases, National Institutes of Health, Bethesda, Maryland 20014. Dr. Carrascosa is now at Centro de Biologia Molecular, Universidad Autonoma de Madrid, Canto Blanco, Madrid 34, Spain.

Received August 28, 1978; accepted September 7, 1978.

0091-7419/79/1001-0001$02.30

prohead which undergoes a sequence of maturation reactions to yield the final head. Although their ordering and interdependence have not yet been fully established, T4 maturation reactions include specific cleavage of the structural proteins of the prohead capsoid, as well as of its morphogenetic core; a 15% expansion of the capsid; a marked stabilization; and packaging of DNA [cf. 6, 11]. Several putative in vivo pathways have been proposed [12–14], but none has yet been rigorously established.

However, considerable progress has been made towards elucidation of proteolysis in this system by isolation of the protease and characterization of its activity [15] and by in vitro processing of polyheads [16, 17], which are tubular capsid analogs also composed of the major head protein gp23.‡ These experiments have shown [16, 17] that cleavage of 10,000 daltons from the amino termini of their gp23 molecules enables the polyheads to undergo a radical structural transformation. Its consequences – expansion, stabilization and exposure of the binding sites for the accessory capsid proteins [18] – appear to simulate capsid maturation. However, an understanding of the relationship between cleavage and structural transformation at the molecular level is still lacking. We have addressed this problem by following up our recent observation [19] that the "empty small particles" *(esp)*, which accumulate in cells infected by mutants in gene 17, contain fully cleaved proteins but have an unexpanded surface lattice. By computer image processing of electron micrographs [20, 21] of "giant" capsoids induced by canavanine [22] we identify the significant structural differences between this hexagonal surface lattice and the uncleaved form, represented in 21^- (protease-deficient) proheads. Giant capsoids [23] are elongated variants of the normal prolate icosahedral morphology formed by axial extension [24] and exhibit a different folding of the surface lattice than those assumed by the open-ended polyheads. Insights into the initiation site of protease activity and into the dynamic relationship between the cleavage and expansion transformations are drawn from micrographs of partially transformed 17^- giant particles.

MATERIALS AND METHODS

Culture Techniques

Escherichia coli B^E was host bacterium. Phage mutants T4D.17 (amNG60) and T4D.21 (amE322) were from our laboratory collection. Media and infection conditions were as described [25]. To induce giant particle formation by canavanine [22], we added 14 μg/ml of L-canavanine to cultures at 4.10^8 bacteria/ml at 11 min postinfection. In labeling experiments, 50 μC of ^{14}C amino acids per ml of culture (Amersham, CFB104) were added at 13 min postinfection and chased 17 min later with casamino acids (final concentration, 1%). Giants from 17^- infections were fixed, either with 4-methylmercaptobutyrimidate [19] or with 0.01% OsO_4, and purified by differential centrifugation. 21^- giants were also purified in this way and (with identical results) as described [16] for polyheads, *esps* were labeled and purified as described [19].

Polyacrylamide Gel Electrophoresis

Gradient acrylamide gels (10–15%) were prepared as described [19]. The immunological test to detect the cleaved fragment of gp23 was performed by the immunoreplicate technique [26] with sera kindly provided by L. Onorato.

‡"gp23" Denotes the product of gene 23; "gp23*" is the cleaved form of this protein [6].

Electron Microscopy and Optical Diffraction

Viral particles were prepared and observed as described [27]. To remove the core structure of 21⁻ giants, the particles were incubated with 1% sodium phosphotungstate [28]. Magnifications were calibrated as described [24]. Optical diffraction patterns, obtained as described [27, 29], were indexed according to previously defined conventions [16].

Image Processing was carried out using a system of programs [21] implemented on the IBM 370/158 computer of F. Hoffman-LaRoche, Basel. Images were digitized as described [29] at a sampling rate of $(0.43\ \text{nm})^{-1}$, and photographic negatives were obtained from digital filtered images as described [9]. Methods for optimizing sampling of the digital Fourier transforms were as described [20]. Filtration of hexagonal reciprocal lattices was basically according to Smith and Aebi [30], except that the filtrations were restored to their original coordinate frames by inverse linear transformation effected by bilinear interpolation. All filtrations were carried out on 30 "super-unit cells" [30] each of dimensions 26 × 44 samples, containing two hexamers. All filtrations were normalized to zero mean density, and to contain the same power. "Average" filtrations were obtained by summation, followed by renormalization, and combined with the individual filtrations to yield the "standard deviation" images. The "difference picture" analysis employed an algorithm that we have described in detail elsewhere [31]. In brief, the algorithm functions by first locating those portions of the respective unit cells where the corresponding densities differ most, and then linearly transforming the pictures to minimize the difference between the remaining areas in a least-squares sense. The pictures are then subtracted. The algorithm has been thoroughly tested for stability and by model experiments [31].

RESULTS

Protein Composition of Particles Produced in 21⁻ and 17⁻ Canavanine-Treated Infections

The particles partially purified from lysates of these cells were analyzed by gel electrophoresis (Fig. 1). As expected for the protease-deficient mutant, the structural proteins of the 21⁻ particles are uncleaved. On the other hand, the gel pattern reveals substantial cleavage in 17⁻-derived particles, indicating that under these conditions canavanine inhibits [32], but does not abolish cleavage. The percentage of gp23 cleaved to gp23* was somewhat variable in the range 50–70%, over repeated experiments. Purified *esps* were also analyzed by electrophoresis to test for the possible presence in these particles of the N-terminal moieties of the gp23 molecules cleaved to gp23*. If intact, these polypeptides would have a molecular weight around 10,600 [33]. The results show no evidence for such a polypeptide or for a smaller fragment. Furthermore, analysis of the gels by the sensitive immunoreplicate technique [26] with antiserum against gp23 showed no indication of any antigen migrating in that zone of the gel.

Structural Characterization of Giant Particles From 21⁻ and 17⁻ Canavanine-Treated Infections

21⁻Canavanine Giants. The giants obtained from 21⁻ lysates (Figs. 2a, 2c) have a coarse-textured appearance in negative stain, very similar to that of "coarse" polyheads [eg, 27], which are also present in these preparations. In what follows, we refer to this capsoid type as "21⁻Can giants."

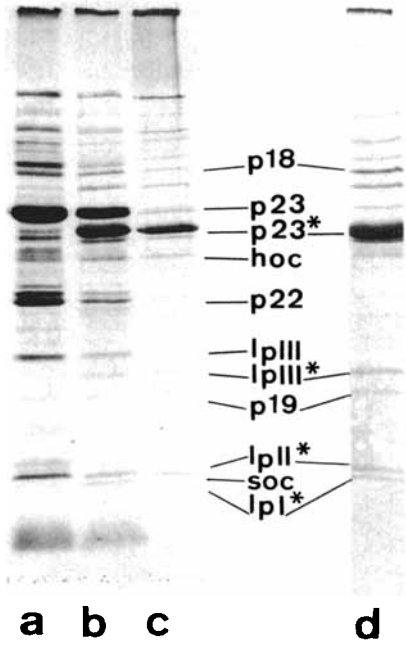

Fig. 1. Structural proteins of 21⁻ and 17⁻ giants. Giant particles (labeled and partially purified as described in Materials and Methods), were analyzed on 10–15% gradient acrylamide gels [19]. Autoradiography of (a) 21⁻-derived giants and (b) 17⁻-derived giants. Purified T4 phage (c) mark the positions of the cleaved proteins. (d) Shows an autoradiogram of labeled purified *esps*. This gel was dried directly to avoid any loss of low molecular weight material by washing while staining.

17⁻ Canavanine Giants. The particles obtained from 17⁻ lysates are also a mixture of giants and coarse polyheads. These giants fall into three different classes [19]. The first class comprises particles whose fine structure, determined by optical filtrations (data not shown), is indistinguishable from the mature giant T4 capsid [1°, 20, 34]. Giants of the second class are seemingly identical to 21⁻ Can giants. The third class of giant (Figs. 2b, 2d) closely resembles the 21⁻Can giants, but optical diffraction patterns from well-preserved particles reveal a clear distinction (Fig. 2e vs Fig. 2f). In both cases, the second radial order of diffraction spots is dominant, but whereas the next strongest order from 21⁻Can giants is the fourth, these spots are very weak for the other type, whose secondary diffraction order is the fifth. In the following, we shall refer to this third class as "17⁻ Can giants." We have only observed such particles in lysates in which substantial cleavage of gp23 has taken place, and we interpret them to be giant *esps* having a cleaved surface lattice. The validity of this correlation is assessed in the Discussion section.

Fine structure of 21⁻Can and 17⁻Can Giants. On the basis of the quality of their diffraction patterns, we selected the five best-preserved giants of both classes and analyzed their fine structures by computer filtration. The detail visualized in the filtered images was highly reproducible within each class. To put this reproducibility on a quantitative basis, we formed the average filtrations from both series (Figs. 2g, 2h) and computed "standard deviation pictures" (Figs. 2i, 2j). In the latter, the departures from the background gray level represent the fluctuations, among the different filtrations, of the detail present at the corresponding points of the respective unit cells. These fluctuations are very slight, amounting at most to 8% (darkest), and on average to 4%, of the optical density range spanned in the

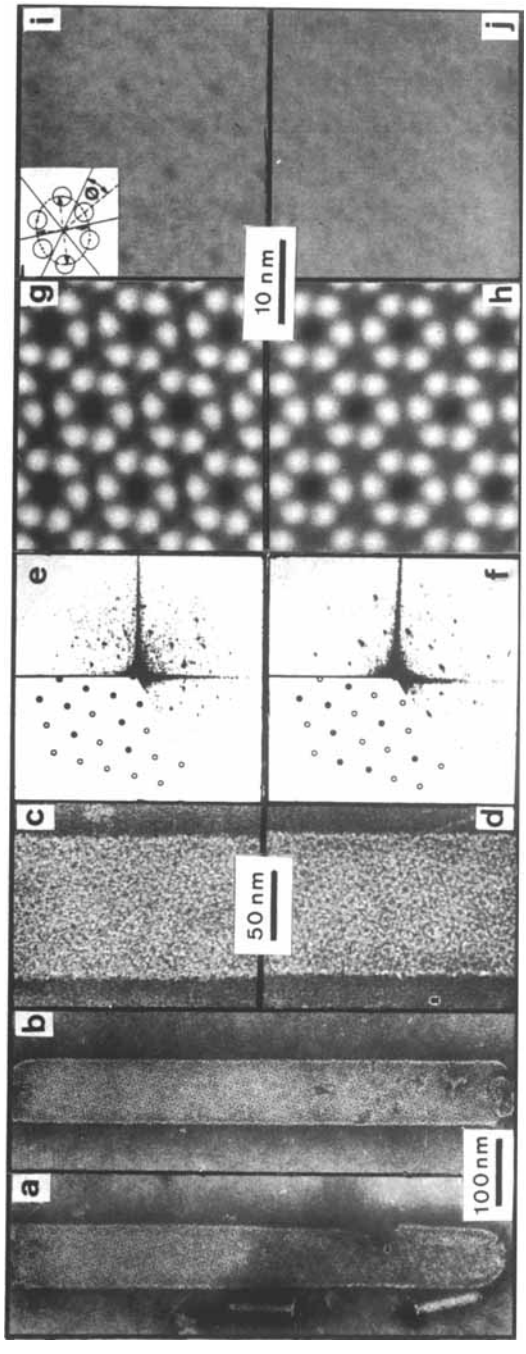

Fig. 2. Giant particles derived from 21^- and 17^- infected cells. Figures (a) and (b) are electron micrographs of 21^-Can and 17^-Can giants stained with 2% sodium phosphotungstate; at higher magnification, (c) and (d). The respective optical diffraction patterns are shown in (e) and (f). Indexation of the hexagonal reciprocal lattices is given in the upper left-hand third of each panel. Reproducibly visible diffraction orders are represented by full circles, and empty circles denote lattice points occupied by weak or invisible diffraction orders. Each diffraction pattern contains two reciprocal lattices derived respectively from the upper and lower surfaces of the flattened particles. These lattices are related by reflection in the vertical axis. For simplicity, only one lattice is indexed in each case. Frames (g) and (h) show respectively computer-filtered images of the 21^-Can and 17^-Can surface lattices. These images each represent the average of five individual filtrations. The fluctuations observed within these two series are represented in the corresponding "standard deviation" pictures (i) and (j) (cf Materials and Methods and Results). The inset to panel (i) shows a schematic hexamer in which the capsomer orientation angle (ϕ) is defined.

filtrations themselves, and emphasize the high degree of reproducibility within the two series of filtrations.

For both classes of giants (Figs. 2g, 2h), we visualize a hexameric capsomer with a diameter (cf Fig. 2i, inset) of 7.5 nm, which has a heavier accumulation of stain at the capsomer center than between capsomers. This distinction underlines the more quantitative nature of computer image processing: our optical filtrations did not detect it and were unable to distinguish the threefold centers from the sixfold centers of the 17.⁻Can surface lattice. The 21.⁻Can hexamer has a greater ellipticity than the almost circular 17.⁻Can hexamer. In addition, the arrangement of its stain-excluding units shows a pronounced clockwise vorticity, in distinction to the 17.⁻Can morphology. These differences, although subtle, are reproducible and are quantitated in Table I. However, the most striking difference is between the respective capsomer orientation angles (cf Fig. 2k) which we determine to be 9.6° for 21.⁻Can giants as opposed to 3.5° for 17.⁻Can giants.

"Difference Picture" analysis between 21.⁻Can and 17.⁻Can capsomer morphologies. In order to detect those locations in the unit cell where the distribution of stain-excluding matter differs most strongly between the respective morphologies, we performed a quantitative "difference picture" analysis between the two average filtrations (Fig. 3). The difference picture obtained by algorithmic subtraction is shown in Fig. 3c. Those features of this image that rise above the highest level of fluctuations represented in the "standard deviation" pictures described above, are shown as white in Fig. 3d. They amount to six symetrically located regions of strain-excluding matter whose locations within the 21.⁻Can unit cell are contoured in Fig. 3e.

In vitro expansion of 17.⁻Can Giants. We have previously shown that incubation at low ionic strength causes *esps* to transform in vitro into expanded capsid-like particles [35]. Under these conditions, unfixed 17.⁻Can giants disappear to be replaced by wider giants with a much smoother appearance. These transformed giants have an expanded surface lattice (cf Table I) and their fine structure (Fig. 4d) is indistinguishable from that of T2L.Can giant capsids [18, 20]. In contrast, 21.⁻Can giants do not transform but simply dissociate when subjected to these conditions.

TABLE I. Surface Lattice Parameters of 21.⁻Can and 17.⁻Can Giant Particles

Type	Lattice constant (nm)	Pitch angle[a]	Particle width (nm)	Capsomer diameter[b] (nm)	Capsomer ellipticity[b]	Capsomer orientation angle[c]
21.⁻Can	11.3 ± 0.3	13.9 ± 0.9°	99.9 ± 3.3	7.5 ± 0.1	1.15 ± 0.03	9.6 ± 0.7°
17.⁻Can	11.2 ± 0.1	14.0 ± 0.5°	95.6 ± 2.1	7.5 ± 0.1	1.04 ± 0.02	3.5 ± 0.5°
In vitro transformed 17.⁻Can	12.8 ± 0.3	13.7 ± 0.6°	107.4 ± 2.3	8.7	1.10	21.1°

[a] Measured as the angle between the meridian and the closest reciprocal lattice line.

[b] Average capsomer diameter $d = (d_1 \cdot d_2)^{1/2}$, d_1 and d_2 being the major and minor axes, respectively, of the ellipse fitted in the capsomer [27] (Fig. 2i, inset): the ellipticity is $e = d_1/d_2$.

[c] The angle between the line connecting the centers of mass of opposite protomers in a hexamer and a lattice line (cf Fig. 2i, inset).

The number of measurements was five in every case except for the capsomer parameters of in vitro transformed 17.⁻Can, whose single measurement tallied with data previously published for T2L.Can giants [20].

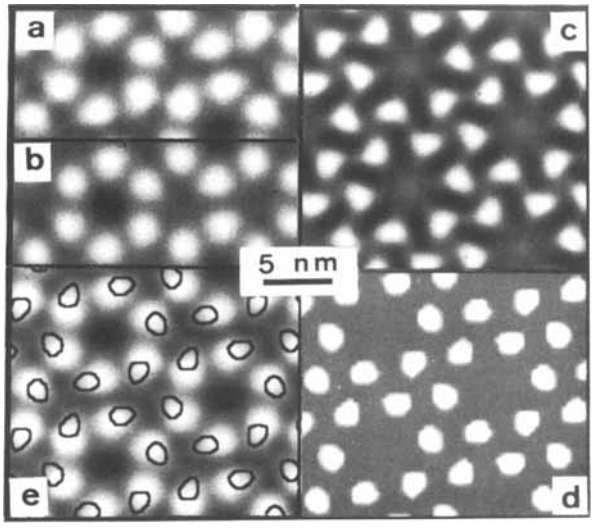

Fig. 3. Difference picture analysis between 21.⁻Can and 17.⁻Can capsomers. The average filtrations of the 21.⁻Can and the 17.⁻Can capsomers, shown in (a) and (b), were used in this analysis. The differences in stain-excluding matter between these capsomers, as detected by algorithmic subtraction (cf. Materials and Methods, Results) are shown in (c). Those densities lower in absolute value than the fluctuations observed between different filtrations of the same class (quantitated as standard deviations) are set in (d), to the background grey level, leaving the significantly different areas as white (stain-excluding matter). Their locations in the 21.⁻Can unit cell are contoured in (e).

Partially transformed ("intermediate") giant particles. In 17.⁻Can lysates, we observe very rare giants on which part of the capsid is in the expanded conformation, while the remainder is unexpanded. An electron micrograph of such a particle is shown in Fig. 4b. In all cases (eight unambiguous examples out of many hundreds of giants observed), the expanded region extends from one cap to merge continuously with the unexpanded region in a sharp band (Transition II in Fig. 4c) about 20 nm in width. This band is oriented quasi-perpendicular to the particle axis: probably the transition front follows the near-equatorial lattice line. The unexpanded region of the giant shown in Fig. 4b was uniformly flattened and well stained. The diffraction pattern generated by the area immediately adjacent to the expanded portion was of the 17.⁻Can type, whereas that generated by the distal region clearly corresponded to the 21.⁻Can morphology, indicating that three successive sectors of the particle were in different structural states. To examine the interface between the latter two regions (Transition I in Fig. 4c), we made a series of filtrations along the particle of which some examples are shown in Figs. 4 e–g. These data are represented in Fig. 4a in terms of the capsomer orientation angles (Fig. 2i, inset), measured from these filtrations. The averaged orientation angle from a transitional area will assume an intermediate value closer to that of the predominant capsomer type. Plotted in Fig. 4a in register with the particle, the data reveal a smooth transition zone extending over some 180 nm after which no significant proportion of 17.⁻Can capsomers is detected. This conclusion was confirmed by determining the axial dependence of a different parameter which distinguishes the two structural states. The picture elements (F_i) of each filtration were expressed as a linear combination of those of the two reference capsomers (C_i and U_i, respectively shown in Figs. 2g and 2h: $F_i = \lambda C_i + (1 - \lambda) U_i$) and the maximum likelihood value of the single

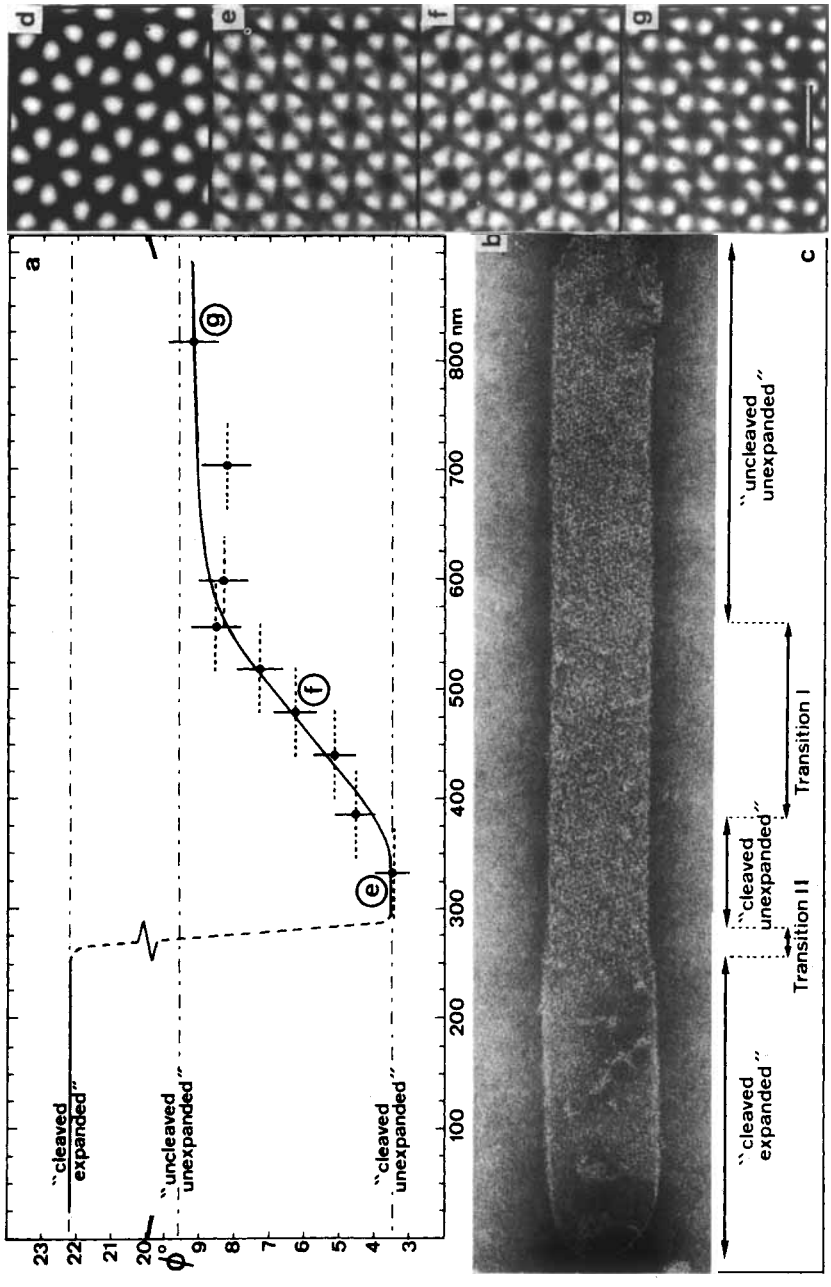

Fig. 4. Partially transformed 17.7 Can giant. The left-hand (wider) end of this particle exhibits the expanded surface lattice conformation. The remainder of the particle is unexpanded and relatively coarse-textured. Its structure has been analyzed, section by section, by computer filtration, of which several examples – (e) to (g) – are shown, together with a filtered image (d) from an in vitro expanded giant. (The calibration bar in (g) represents 10 nm.) These data are summarized (a) by plotting the axial dependence along the particle of the orientation angle of the hexameric capsomer. The broken lines (– · – · –) mark the orientation angle values characteristic of "cleaved, unexpanded," "uncleaved, unexpanded," "cleaved, expanded" giant capsoids. The error bar values were taken from the standard deviations recorded in these sets of measurements. The dashed lines (– – –) on data points indicate the particle areas contributing to the corresponding filtered images.

parameter λ determined by least-squares solution. The reference pictures of the two states correspond to the values $\lambda = 0$ and $\lambda = 1$, respectively, and fractional values correspond to intermediates varying between these two extremes. No significant difference showed up between this curve (data not shown) and the ϕ-trajectory shown in Fig. 4a.

DISCUSSION

Correlation Between Cleavage of gp23 and Capsomer Morphology

We have made a structural analysis of giant head-related particles partially purified from canavanine-treated T4.21$^-$ and T4.17$^-$ infections, and analyzed their protein compositions. No cleavage was registered in the 21$^-$ particles, whose surface lattice therefore contains gp23. In 17.$^-$Can lysates, substantial proportions (50–75%) of gp23* were detected, of which a certain amount is accounted for by the giant mature capsids present. Of the two morphological types of unexpanded giant present in 17.$^-$Can lysates, the first is indistinguishable from 21.$^-$Can giants. Presumably, together with contaminating polyheads they contribute the fraction of uncleaved protein. We correlate the different capsomer morphology of the second class (17.$^-$Can giants) with the presence of gp23* in their surface lattices on the following grounds:

1) The 17.$^-$Can giant is never observed in the absence of cleavage.

2) It has the same lattice constant, appearance, and genetic origin as the gp23*-containing *esp* [19].

3) Like the *esp*, the 17.$^-$Can giant can be expanded in vitro, under conditions that dissociate both 21$^-$ proheads and 21.$^-$Can giants.

In the light of this evidence, we assume that the 17.$^-$Can giants are derived from the *esp* by abnormal elongation caused by the influence of canavanine.

Comparison with polyhead studies. The capsomer structure of 21.$^-$Can giants is very similar to that of uncleaved, unexpanded polyheads, except that its ellipticity is slightly less accentuated than in polyheads [27]. The properties of the 17.$^-$Can giants suggest a relationship with the "cleaved but anchored" polyheads observed by Laemmli et al [17]. However, the most pronounced difference between the fine structures of the uncleaved and cleaved forms of unexpanded surface lattice in giant capsoids lies in the capsomer orientation angles, which we determine to be 9.6° and 3.5° respectively. These results are not in agreement with those of Laemmli et al [17], who reported an increase in orientation angle from 13–15° to 15–18° upon conversion of uncleaved polyheads to the "cleaved but anchored" form.

Cleavage-related change in capsomer morphology. The significant differences between the 21.$^-$Can and 17.$^-$Can unit cell morphologies (Fig. 3), amount to six equivalently located portions of stain-excluding matter. Their removal from the uncleaved hexamer image accounts for the change in orientation angle and vorticity observed in the cleaved hexamer. Thus, it is tempting to equate these features with the locations within the uncleaved unit cell of the amino-terminal portions of the gp23 monomers. In the following, we evaluate the evidence which bears on this proposition.

1) Is the N-terminal portion of gp23 removed upon cleavage? Electrophoresis of purified *esps* shows no indication of an unaccounted candidate polypeptide. Multiple cleavage events might possibly generate smaller polypeptides undetected by our gels which could remain associated with the particle.However, we feel this to be unlikely, since examination of phage and cell extracts [36, 37] have afforded no evidence of any such gp23-derived peptide.

2) Structural additivity or allosteric change? The remarkable similarities between the two surface lattices, coupled with the fact that the significantly different features are so localized, encourage the hypothesis that these parts (Fig. 3c) of the uncleaved capsomer might be associated with the amino-terminal portions of gp23 monomers. However, our filtrations depict only projections of stain-excluding matter, and specific molecular features cannot be identified from them. This change in capsomer morphology can be explained equally plausibly by allosteric rearrangement, of which a striking example is represented by the expansion transformation to which the cleaved surface lattice is susceptible. Experiments to detect antigenic differences (J.L.C., work in progress) may help to clarify this point.

Relationship between cleavage and expansion. In vitro studies on polyheads [16, 17] have shown that cleavage of gp23 facilitates a stabilizing expansion of the surface lattice. The same holds true for the giant capsoids studied here. Our data are consistent with the suggestion [17, 19] that immediate expansion is not an obligatory consequence of cleavage, which creates an intermediate state that subsequently can be provoked to expand. The alternative decoupling of expansion and cleavage has been observed in particles from the mutant 23(tsA78) which were found to be expanded and yet to contain uncleaved gp23 [38]. However, at the nonpermissive temperature this mutant exhibits abnormal assembly properties [39]; no viable phages have yet been found which contain gp23 uncleaved.

Dynamics of structural transformation. In 17 Can lysates, we have detected a few giants expanded at one end only. On one well-preserved example permitting detailed analysis (Fig. 4), the unexpanded region was found to contain a diffuse zone of partial cleavage, separating fully cleaved and uncleaved sectors. In contrast, the transition between the expanded end and the remainder of each particle (as in all other cases observed) was sharp although structurally continuous. The paucity of these data does not allow definitive conclusions to be drawn about the dynamic progress of the cleavage and expansion transformations. Nevertheless, in conjunction with our earlier observations [16] on partially transformed polyheads, they suggest that the transformations proceed along the following lines:

1) The cleavage pattern is polar, initiating in one end-cap, and propagating along the particle to create an intermediate state of the surface lattice.

2) The expansion transformation is also polar, triggered in an end-cap, and progresses rapidly, irreversibly, along the particle in a cooperative transformation comparable to contraction of the phage tail sheath during infection [40].

ACKNOWLEDGMENTS

We gratefully acknowledge Dr. P.R. Smith for guidance in the computer program system developed by him, Professor E. Kellenberger in whose laboratory this work was performed, Drs. R. van Driel and J. Kistler for helpful criticism of the manuscript, Drs. K. Seidel and A. Funkhouser (ETH, Zürich) for photo-writing facilities and the EDV Department of Hoffman-La Roche, Basel, for generous provision of computing facilities. This work was supported by grants from the European Molecular Biology Organization (to J.L.C.) and the Swiss National Foundation (to Professor E. Kellenberger).

REFERENCES

1. Neurath H, Walsh KA: Proc Natl Acad Sci USA 73:3825–3832, 1976.
2. Reich E, Rifkin D, Shaw E (eds): Cold Spring Harbor Laboratory, Cold Spring Harbor, New York, 1975.

3. Inouye S, Wang S-S, Sekizawa J, Halegoua S, Inouye M: Proc Natl Acad Sci USA 74:1004–1008, 1977.
4. Inouye HC, Beckwith J: Proc Natl Acad Sci USA 74:1440–1444, 1977.
5. Hershko A, Fry M: Ann Rev Biochem 44:775–797, 1975.
6. Casjens S, King J: Ann Rev Biochem 44:555–611, 1975.
7. Dickson R, Barnes S, Eiserling FA: J Mol Biol 53:461–473, 1970.
8. Hosoda J, Cone R: Proc Natl Acad Sci USA 66:1275–1281, 1970.
9. Kellenberger E, Kellenberger C: FEBS Lett 8:140–144, 1970.
10. Laemmli UK: Nature 227:680–685, 1970.
11. Showe MK, Kellenberger E: In Burke DC, Russell WC, (eds): "25th Symposium of the Society of General Microbiology." Cambridge University Press, 1975, pp 407–439.
12. Laemmli UK, Favre M: J Mol Biol 80:575–599, 1973.
13. Kellenberger E: In Nover L, Mothes K (eds): "Cell Differentiation in Microorganisms, Plants and Animals." Elsevier, Amsterdam, 1977, pp 317–339.
14. Hsiao CL, Black LW: Proc Natl Acad Sci USA 74:3652–3656, 1977.
15. Showe MK, Isobe E, Onorato L: J Mol Biol 107:35–54, 1976.
16. Steven AC, Couture E, Aebi U, Showe MK: J Mol Biol 106:187–221, 1976.
17. Laemmli UK, Amos L, Klug A: Cell 7:191–203, 1976.
18. Ishii T, Yanagida M: J Mol Biol 97:655–660, 1975.
19. Carrascosa JL, Kellenberger E: J Virol 25:831–844, 1978.
20. Aebi U, Bijlenga RKL, ten Heggeler B, Kistler J, Steven AC, Smith PR: J Supramol Struct 5:475–495, 1976.
21. Smith PR: Ultramicroscopy 3:153–160, 1978.
22. Cummings DJ, Chapman VA, DeLong SS, Couse NL: Virology 54:245–261, 1973.
23. Doermann AH, Eiserling FA, Boehner L: J Virol 12:374–385, 1973.
24. Aebi U, Bijlenga R, van den Broek J, van den Broek R, Eiserling FA, Kellenberger C, Kellenberger E, Mesyanzhinov V, Müller L, Showe MK, Smith PR, Steven AC: J Supramol Struct 2:253–275, 1974.
25. Bijlenga RKL, Scraba D, Kellenberger E: Virology 56:250–267, 1973.
26. Showe MK, Isobe E, Onorato L: J Mol Biol 107:55–69, 1976.
27. Steven AC, Aebi U, Showe MK: J Mol Biol 102:373–407, 1976.
28. Van Driel R, Couture E: J Mol Biol 123:115–128, 1978.
29. Aebi U, Smith PR, Dubochet J, Henry C, Kellenberger E: J Supramol Struct 1:498–522, 1973.
30. Smith PR, Aebi U: J Supramol Struct 5:493–495, 1977.
31. Carrascosa JL, Steven AC: Mioron (in press).
32. Bolin RW, Cummings DJ: J Virol 13:1378–1391, 1974.
33. Tsugita A, Black LW, Showe MK: J Mol Biol 98:271–275, 1975.
34. Bijlenga RKL, Aebi U, Kellenberger E: J Mol Biol 103:469–498, 1976.
35. Carrascosa JL: J Virol 26:420–428, 1978.
36. Eddleman HL, Champe SP: Virology 30:471–481, 1966.
37. Giri JG, McCullough JE, Champe SP: J Virol 18:894–903, 1976.
38. Onorato L, Showe MK: Experientia 33:1683–1684, 1977 (Abstr).
39. Favre R, Boy de la Tour E, Segre N, Kellenberger E: J Ultrastruct Res 13:318–342, 1965.
40. Moody MF: J Mol Biol 80:613–625, 1973.